Emergent Properties of Convection in OTREC and PREDICT

D. J. Raymond[1] and Ž. Fuchs-Stone[1]

[1]Physics Department and Climate and Water Consortium
New Mexico Tech
Socorro, NM 87801 USA

Key Points:

- Observations of emergent properties of convection from the OTREC and PREDICT field programs are reported.
- Column relative humidity, low to mid-tropospheric moist convective instability, and convective inhibition govern moisture convergence.
- Top-heavy mass flux profiles and moist entropy divergence increase with increasing sea surface temperature.

Corresponding author: David Raymond, david.raymond@nmt.edu

Abstract

Gridded dropsonde analyses are made using data from the OTREC (Organization of Tropical East Pacific Convection) and PREDICT (Pre-Depression Investigation of Cloud-Systems in the Tropics) projects to characterize the mesoscale properties of tropical oceanic convection in terms of selected thermodynamic parameters computable from the explicit grids of large-scale models. In particular, column relative humidity, low to mid-tropospheric moist convective instability, and convective inhibition correlate with moisture convergence, while sea surface temperature is related to the top-heaviness of mass flux profiles and the integrated entropy divergence. Local (as opposed to global) surface heat and moisture fluxes and convective available potential energy have little relation to these quantities. These results provide useful constraints for cumulus parameterizations.

Plain Language Summary

Observations of the atmosphere from two field programs over tropical oceans are used to determine the characteristics of rain-producing clouds in these regions. In particular we are interested in what types of temperature and humidity profiles in the atmosphere promote rainfall and which types suppress it. This information is useful in designing and testing of treatments of clouds and rain in global weather and climate models. As a result of this research, we present a set of recommendations to modelers involved in this work.

1 Introduction

Representing deep convection in global weather and climate models with sufficient fidelity is a problem that has eluded solution for many decades. This lack of progress is a significant impediment to extending long-range weather forecasts beyond their current limits and is one of the main sources of uncertainty in climate models.

Traditional parameterizations of convection in global models fall into two broad categories. Reductionist schemes attempt to build on our knowledge of the fundamental elements that are thought to work together to form ensembles of convection, e.g., plumes, thermals, cold pools, etc. More empirical schemes try to infer emergent properties of such ensembles that are less dependent on our knowledge of such nuts and bolts.

Most reductionist schemes focus on the representation of convective updrafts as plumes, with some quasi-equilibrium principle controlling the number and size distributions of updrafts. Other aspects of convection such as downdrafts and stratiform rain areas are often treated in an ad hoc fashion. An early and enduring example of such a "mass flux" scheme is that of *Arakawa and Schubert* [1974] (see also *Arakawa* [2004]). There are many derivatives of this scheme. In the original version, updrafts are represented by a spectrum of plumes, with the strength of each plume size governed by an equilibrium between the plume-specific consumption of conditional instability and its generation by non-convective processes. Only in *Cheng and Arakawa* [1997] were downdrafts added to the original Arakawa-Schubert scheme. The effects of stratiform rain areas, which contribute significantly to the precipitation total [*Zipser*, 1969; *Zipser*, 1977; *Houze and Cheng*, 1981; *Houze*, 1989; *Houze*, 2004], are generally ignored.

The convective adjustment schemes of *Manabe et al.* [1965], *Betts* [1986], *Betts and Miller* [1986], *Betts and Miller* [1993], *Raymond* [2007] etc., are empirical convective parameterizations and are based on the hypothesis that the main effects of deep convection can be represented via mixing in response to moist convective instability, with the additional proviso that condensed water resulting from the mixing is precipitated out. Though currently not much used for various reasons, some of these models produce remarkably good simulations of the global circulation and the Madden-Julian oscillation

(MJO), given their simplicity [*Hayashi and Golder*, 1997a; *Hayashi and Golder*, 1997b; *Raymond*, 2001; *Raymond and Fuchs*, 2009].

The advance in computing power has opened new opportunities in the area of cumulus parameterization. Of particular interest is the use of a small cloud-resolving model in each global model grid box in place of a conventional cumulus parameterization [*Grabowski*, 2001; *Grabowski*, 2003; *Khairoutdinov and Randall*, 2001; *Khairoutdinov et al.*, 2005]. By themselves, these superparameterized models are too computationally intensive to be run routinely for long periods or at high spatial resolution. However as *Benedict and Randall* [2009] have shown, a superparameterized model is capable of reproducing the MJO with better fidelity than virtually all models with reductionist convective parameterizations.

In a more indirect approach, *Rasp et al.* [2018] used data from a global aquaplanet model employing a superparameterization of convection to train a deep neural network to produce heating and moistening profiles in each grid box that are consistent with the outputs of the embedded convective models. The trained neural network works with the global model to produce results that are very close to those of the original superparameterized model at a much lower computational cost. Computations driven by the neural network with boundary conditions that deviate from the training regime also are close to superparameterized calculations as long as the calculations don't go outside the phase space of the original training data set.

Recent observations of deep tropical convection using grids of dropsondes deployed from high altitude [*Elsberry and Harr*, 2008; *Montgomery et al.*, 2012; *Braun et al.*, 2016; *Fuchs-Stone et al.*, 2020] provide an additional opportunity to improve convective parameterizations. Though incapable of revealing the structure of individual convective cells, such observations can be used to document the mesoscale structure of convective ensembles along with budgets of heat, moisture, and momentum. The environment of convection can also be documented, thus in principle providing all the information needed to understand how convective ensembles interact with their environment. Recent studies of this kind include *Raymond et al.* [2011], *Gjorgjievska and Raymond* [2014], and *Juračić and Raymond* [2016].

In this paper we present a framework for using observations of the type described above to test thermodynamic parameterizations of convection for use in large-scale models. We base these results on a comparative study of two very different field programs, PREDICT2010 (Pre-Depression Investigation of Cloud-Systems in the Tropics; *Montgomery et al.* [2012]) and OTREC2019 (Organization of Tropical East Pacific Convection; *Fuchs-Stone et al.* [2020]). The former studied convection in cloud systems with potential to develop into tropical cyclones in the Western Atlantic and Caribbean, while the latter examined convection in the East Pacific Intertropical Convergence Zone (ITCZ) as well as the Pacific coastal region of Colombia and the far Southwest Caribbean. PREDICT experienced generally higher sea surface temperatures (SSTs) than OTREC as well as stronger vorticities due to higher latitudes and the prevalence of tropical cyclone precursors.

Though the results from OTREC and PREDICT differ in detail, they share the main features, namely that three parameters promote larger values of vertically integrated moisture convergence and hence mean rainfall. These are larger saturation fraction (a kind of column-integrated relative humidity), smaller but non-negative instability index (low to mid-tropospheric moist convective instability), and smaller deep convective inhibition (ascending parcel consists of a mixture of air from the lowest kilometer). Furthermore, higher SSTs result in more top-heavy mass flux profiles and larger vertically integrated moist entropy divergence. Local (as opposed to broad area) surface heat and moisture fluxes and convective available potential energy are less important. These emer-

gent properties of convection are likely to be useful in the development and testing of cumulus parameterizations.

Section 2 introduces the theoretical background. Analysis methods used on OTREC and PREDICT data are documented in section 3 while section 4 presents the results of these analyses. Section 5 discusses lessons learned for cumulus parameterizations and conclusions are presented in section 6.

2 Theoretical basis

All global models have at least two thermodynamic equations, one for the moisture and another for the energy or moist entropy. Different models define different combinations of variables, but they are ultimately equivalent.

2.1 Fundamental relationships

We present equations for these two variables in geometrical height coordinates. The precise water variable is the total cloud water, or water vapor plus advected condensate mixing ratio, r_t. The specific moist entropy, including ice processes, is represented by s, which is defined by *Raymond* [2013] as

$$\begin{aligned} s &= (C_p + rC_{pv} + r_l C_l + r_i C_i)\ln(T/T_F) - \\ &\quad R_d \ln(p_d/p_R) - rR_v \ln(p_v/e_{SF}) + \\ &\quad \frac{Lr - L_F r_i}{T_F} \end{aligned} \tag{1}$$

where C_p and C_{pv} are the specific heats of dry air and water vapor at constant pressure, C_l, and C_i are the specific heats of liquid water and ice, and R_d and R_v are the gas constants for dry air and water vapor. The quantity T is the temperature, p_d and p_v are the partial pressures of dry air and water vapor, r is the water vapor mixing ratio, and r_l and r_i are the mixing ratios of liquid water and ice. The constants are the freezing point of water T_F, a constant reference pressure $p_R = 10^5$ Pa, the saturation vapor pressure at freezing for water vapor e_{SF}, the latent heat of condensation at freezing L, and the latent heat of freezing L_F. This expression assumes that $r_i = 0$ for $T > T_F$ and $r_l = 0$ for $T < T_F$.

The total cloud water equation in flux form is

$$\frac{\partial \rho r_t}{\partial t} + \nabla \cdot (\rho \mathbf{v} r_t) + \frac{\partial}{\partial z}(\rho w r_t + F_t) = -\rho P \tag{2}$$

where ρ is the air density, ∇ is the horizontal gradient operator, $(\mathbf{v}, w)$ are the horizontal and vertical components of air velocity, F_t is the vertical eddy flux of r_t, including surface evaporation at $z = 0$, F_{ts}, and P the specific conversion rate of cloud water to precipitation. The entropy obeys a similar equation

$$\frac{\partial \rho s}{\partial t} + \nabla \cdot (\rho \mathbf{v} s) + \frac{\partial}{\partial z}(\rho w s + F_s) = \rho R/T \tag{3}$$

where F_s is the eddy flux of moist entropy with surface value F_{ss}, T is the temperature, and R is the specific radiative heating rate (generally negative). Several approximations are made in (2) and (3). In particular, horizontal eddy fluxes are ignored, as is the irreversible generation of entropy. They are also incomplete in that models for the precipitation and radiation terms are needed, as is a means of estimating surface fluxes F_{ts} and F_{ss}. In addition, the anelastic mass continuity equation

$$\nabla \cdot (\rho \mathbf{v}) + \frac{\partial \rho w}{\partial z} = 0 \tag{4}$$

is needed.

Considerable information can be extracted from vertical integrals, represented by square brackets [ ], of these equations. Assuming that $w = 0$ at the surface and the upper bound of the integral, (2) can be written

$$[\rho P] = -\nabla \cdot [\rho \mathbf{v} r_t] + F_{ts} - \frac{\partial [\rho r_t]}{\partial t}. \tag{5}$$

If the time derivative can be ignored, this expresses the well-known result that the precipitation rate equals the vertically integrated moisture convergence plus the surface evaporation rate. The time dependence is generally important, but in statistical averages it may be possible to neglect this term.

A similar analysis of (3) yields

$$\frac{\partial [\rho s]}{\partial t} = -\nabla \cdot [\rho \mathbf{v} s] + [\rho R/T] + F_{ss}. \tag{6}$$

Thus, in principle the time tendency of the column-integrated moist entropy can be computed. *Juračić and Raymond* [2016] found this measure to be useful in predicting the tendency of a tropical cyclone to intensify or decay.

An estimate for the time tendency of column cloud water may be extracted on the basis of three assumptions. First we use an approximate form of the moist entropy (1) that ignores liquid and ice condensate as well as all but the last term involving the vapor mixing ratio

$$\begin{aligned} s &\approx C_p \ln(T/T_F) - R_d \ln(p/p_R) + \frac{Lr}{T_F} \\ &= s_d + \frac{Lr}{T_F} \end{aligned} \tag{7}$$

where $p = p_d + p_v$ is the total pressure and $s_d = C_p \ln(\theta/T_F)$ is the specific dry entropy, with θ being the potential temperature. Second, we assume that the weak temperature gradient approximation holds, so that the θ profile doesn't change much with time. Third, we assume that $r \approx r_t$. Under these assumptions, we infer that

$$\frac{\partial [\rho r_t]}{\partial t} \approx \frac{T_F}{L} \frac{\partial [\rho s]}{\partial t} \tag{8}$$

[*Raymond*, 2000]. Combining (5) - (8) results in an estimate for the instantaneous precipitation rate

$$[\rho P] \approx F_{ts} + \frac{T_F}{L} (\nabla \cdot [\rho \mathbf{v} s_d] - [\rho R/T] - F_{ss}). \tag{9}$$

This does not depend on a time tendency, which is difficult to measure. Negative values produced by this equation simply indicate that the rainfall rate is zero. In this case

$$\nabla \cdot [\rho \mathbf{v} s_d] = [\rho R/T] + F_{ss} - L F_{ts}/T_F \quad \text{(no rain)}. \tag{10}$$

Over tropical oceans the Bowen ratio is usually small, which means that $T_F F_{ss} \approx L F_{ts}$, which further simplifies (9) and (10).

Surface fluxes are estimated using a bulk flux formula. For a variable χ, the surface flux is defined by

$$F_{\chi s} = \rho_s C_d U_{eff} (\chi_{ss} - \chi_s) \tag{11}$$

where ρ_s is the surface density, $C_d = 0.002$ is the assumed drag coefficient. $U_{eff} = (u_s^2 + v_s^2 + W^2)^{1/2}$ is the effective surface wind with (u_s, v_s) being the actual surface wind and $W = 3$ m s^{-1} being a gustiness factor. χ_s is the surface value of the variable in question and χ_{ss} is the associated sea surface value. For the thermodynamic variables, χ_{ss} is the saturated value at the sea surface temperature and pressure. For wind, $\chi_{ss} = 0$.

The vertically integrated radiative heating ρR plays a similarly small role in these budgets. Since we have no measurements of this quantity, we simply take $T_F[\rho R/T] = -200$ W m^{-2}.

Finally, using elementary thermodynamics, we define an approximate convective available potential energy (CAPE) by

$$\text{CAPE} = \int (s_p^* - s_{env}^*) dT \tag{12}$$

where s_p^* and s_{env}^* are respectively the saturated moist entropy of an ascending parcel and of the environment. The integral is over positive values of the integrand and s_p^* equals the mean moist entropy in the lowest kilometer of the environment.

2.2 Gross moist stability

A central concept in the study of tropical convection is the gross moist stability (GMS). The GMS was introduced by *Neelin and Held* [1987], who developed a model that relates low-level convergence over tropical oceans to the SST. They assume that the moist static energy in the upper troposphere is approximately equal to the dry static energy there, due to the low value of saturation mixing ratio at upper levels. In the steady state, the difference Δm between the moist static energy in the upper and lower troposphere times the upper level divergence $\nabla \cdot \mathbf{v}$ (which is assumed to equal the low-level convergence) must equal the net transfer rate of moist static energy F_{net} into the atmosphere from surface and tropopause turbulent and radiative fluxes, which implies that

$$\nabla \cdot \mathbf{v} = \frac{F_{net}}{\Delta m}. \tag{13}$$

They denote Δm the gross moist stability. They further assume that the upper tropospheric moist static energy is invariant due to the lack of significant free tropospheric horizontal temperature gradients in the tropics, while the lower tropospheric moist static energy increases with SST. As a result, the convergence-divergence doublet in the troposphere, and hence the precipitation rate, increases nonlinearly with SST as Δm becomes smaller, in broad agreement with observed climatology.

The GMS of *Neelin and Held* [1987] is defined in terms of a two-level model. A conceptually similar form applicable to a continuous vertical coordinate is

$$\text{GMS} \equiv \frac{T_F \nabla \cdot [\rho \mathbf{v} s]}{-L \nabla \cdot [\rho \mathbf{v} r_t]} = \frac{\text{entropy divergence}}{\text{moisture convergence}} \tag{14}$$

[*Raymond et al.*, 2009]. The constants T_F and L give the numerator and denominator the units energy per unit area per unit time, making the GMS dimensionless. The terms "entropy convergence" and "moisture divergence", as used subsequently, include these constants.

Using the above definition of GMS, *Raymond* [2000] generalized the results of *Neelin and Held* [1987] to the time-dependent case with an analysis similar to that in section 2.1. If the numerator and denominator of the GMS associated with convection can somehow be specified in terms of environmental parameters, then the ideas of *Neelin and Held* [1987] and *Raymond* [2000] become powerful tools for predicting the amount of convection and the precipitation rate.

2.3 Convective evolution in the GMS plane

Convective systems of all sizes and types over tropical oceans tend to evolve through a life cycle in similar ways. As *Masunaga and L'Ecuyer* [2014], *Inoue and Back* [2015], and *Inoue and Back* [2017] have shown, this life cycle can be represented concisely as

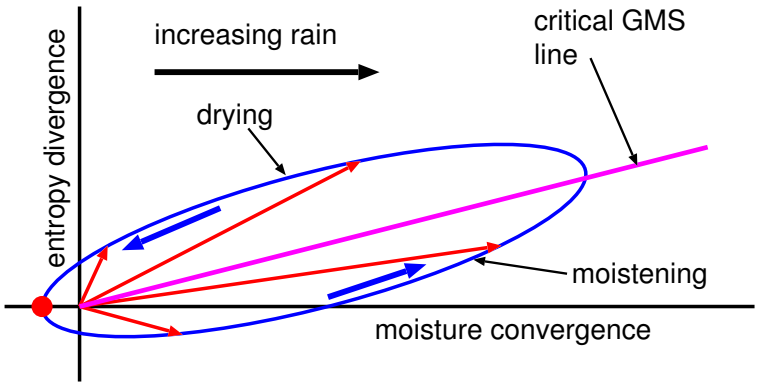

Figure 1. Schematic of GMS plane with the trajectory of a convective life cycle.

a trajectory in the so-called "GMS plane". The horizontal axis of this plane is the column-integrated divergence of dry static energy, or almost equivalently, the column-integrated moisture convergence, $-L\nabla\cdot[\rho\mathbf{v}r_t]$. The vertical axis is the integrated divergence of moist static energy or moist entropy $T_F\nabla\cdot[\rho\mathbf{v}s]$.

Figure 1 shows a schematic of the GMS plane. Convection starts at the red dot on the left and follows the counter-clockwise trajectory defined by the blue line, ending up again at the red dot. The slope of the line from the origin to some point on the trajectory defines the GMS of the system at that point [*Raymond et al.*, 2009].

As a system evolves, it moves from negative values of GMS through increasingly positive values. As *Masunaga and L'Ecuyer* [2014] and *Inoue and Back* [2015] show, the system moistens and rainfall increases up to a critical point and then dries with decreasing rainfall. The slope of the line from the origin through this point is called the "critical GMS" by *Inoue and Back* [2015]. *Masunaga and L'Ecuyer* [2014] and *Inoue and Back* [2015] show that the growing phase of convection is associated with bottom-heavy vertical mass flux profiles, which gradually evolve to top-heavy profiles as the convection peaks and begins to decay. This picture is reminiscent of deep convection in the Asian winter monsoon, as documented by *Churchill and Houze* [1984] and many other studies.

Much work on tropical convection has been focused on squall lines, which are propagating mesoscale systems where the evolution from growing to decaying convection appears to be spatial rather than temporal in a co-moving reference frame [*Zipser*, 1977; *Houze*, 1997; *Churchill and Houze*, 1984; *Houze*, 2004]. However, even in these systems, the evolution of individual convective cells typically looks more temporal than spatial in the earth's reference frame.

2.4 Correlates to strong convection

A great deal of work has gone into documenting the structure and evolution of tropical, oceanic convection. Historically, much less effort has been applied to uncovering the factors that control the prevalence and strength of such convection. However, this has begun to change in recent years.

An important factor known to be associated with tropical oceanic convection is the column relative humidity or saturation fraction, defined as

$$\mathrm{SF} = \int r dp \Big/ \int r^* dp \tag{15}$$

where the integrals are of pressure over the troposphere, r is mixing ratio, and r^* is the saturation mixing ratio [*Sherwood*, 1999; *Bretherton et al.*, 2004; *Raymond et al.*, 2007; *Neelin et al.*, 2009]. Saturation fraction is also thought to be significant in the dynamics of intraseasonal oscillations [*Raymond and Fuchs*, 2009; *Sobel and Maloney*, 2012; *Sobel and Maloney*, 2013; *Kim and Co-Authors*, 2014; *Adames and Kim*, 2016; *Fuchs and Raymond*, 2017].

Early tropical meteorologists understood that the strongest convection and rainfall in the tropics were accompanied by low values of the CAPE [*Ramage*, 1971]. Though this is an association not implying causality, the obvious interpretation is that the convection is causing the decrease in CAPE as it "uses it up". To a certain extent this stands up to critical scrutiny, as convective downdrafts decrease the moist entropy of the boundary layer, thus reducing CAPE. However, on slightly longer time scales, this modification of the boundary layer is countered by surface heat fluxes, which tend to restore the boundary layer to its initial state, typically in less than a day [*Raymond*, 1995]. The other component to CAPE is the buoyancy profile in the free troposphere, which can be reduced by subsidence induced by the convection itself. However, such buoyancy anomalies also rapidly dissipate as the buoyancy is spread over a large area by gravity waves [*Bretherton and Smolarkiewicz*, 1989; *Mapes*, 1993]. More permanent changes in CAPE can only be effected by some mechanism that causes more durable changes in the atmospheric temperature profile.

CAPE as normally defined may not be the best measure of the effect of tropospheric buoyancy on convection. *Kuang* [2008] finds that a "lower tropospheric CAPE" defined as the difference between the boundary layer moist static energy and the saturated moist static energy in the lower half of the troposphere is a more pertinent parameter. In particular, a quasi-equilibrium process exists in which just enough convection is generated to keep this parameter close to a certain value. In addition, for convection to penetrate above the mid-troposphere, the mid-tropospheric relative humidity must be sufficiently high according to *Kuang* [2008].

Raymond et al. [2011] introduced an "instability index" (II) which is related to the lower tropospheric CAPE of *Kuang* [2008]. This is defined by

$$\mathrm{II} = s^*_{lo} - s^*_{hi} \tag{16}$$

where s^*_{lo} and s^*_{hi} are respectively the saturated moist entropy averaged over 1-3 km and 5-7 km. (It differs from the lower tropospheric CAPE in that the boundary layer entropy is not used, only the saturated entropy just above the boundary layer.) Average rainfall tends to be more intense for *smaller*, but non-negative values of II [*Raymond and Sessions*, 2007; *Raymond et al.*, 2014; *Sessions et al.*, 2015; *Sentić et al.* 2015; *Raymond and Flores*, 2016; *Raymond and Kilroy*, 2019]. This result at first appears to be counterintuitive. However, modeling and observation show that smaller II is associated with concentration of mass convergence in a thinner layer near the surface where the mixing ratio tends to be higher. Because of this, a given mass convergence results in stronger moisture convergence and hence more rainfall. *Raymond and Sessions* [2007] demonstrated that the strengthening of precipitation by low values of II is an effect independent of the enhancement of precipitation by increased saturation fraction. Note that the instability index is purely a function of the atmospheric temperature profile since it depends only on temperature and pressure.

A third parameter of interest is a measure of the convective inhibition. The usual measure takes air from a thin surface layer, typically the subcloud layer, and computes the work required to lift such air to the level of free convection. On the hypothesis that deep convection over tropical oceans draws its updraft from a deeper layer, we define a deep convective inhibition index

$$\mathrm{DCIN} = s^*_{th} - s_{bl} \tag{17}$$

where the mean moist entropy of the rising air s_{bl} is the average moist entropy in the lowest kilometer and the threshold entropy s^*_{th} is the saturated moist entropy in a threshold layer, typically taken to be in the 1.5−2 km range [*Raymond et al.*, 2003; *Raymond*, 2017; *Raymond and Kilroy*, 2019].

Models of boundary layer forcing of convection by SST gradients [*Lindzen and Nigam*, 1987; *Battisti et al.*, 1999; *Stevens et al.*, 2002; *Back and Bretherton*, 2009] produce regions of convergence and divergence that are thought to be related to the formation or suppression of convection. Since the vertical velocities associated with this convergence are unlikely to directly affect deep convection, this lifting presumably acts via the resulting destabilization of the lower troposphere which reduces the convective inhibition. This mechanism is therefore likely to be captured by the DCIN parameter.

Tropical oceanic convection has been found to increase with increasing surface latent heat fluxes in observations [*Raymond*, 1995; *Maloney and Esbensen*, 2003; *Maloney and Sobel*, 2004; *Raymond et al.*, 2006] and in models [*Maloney and Esbensen*, 2005; *Raymond and Sessions*, 2007; *Raymond and Flores*, 2016]. This mechanism is thought to be central to the dynamics of tropical cyclones [*Emanuel*, 1986; *Emanuel*, 1995] and intraseasonal oscillations [*Emanuel*, 1987; *Neelin et al.*, 1987; *Raymond*, 2001; *Araligidad and Maloney*, 2008; *Raymond and Fuchs*, 2009; *Fuchs and Raymond*, 2017; *Shi et al.*, 2018; *Khairoutdinov and Emanuel*, 2018]. It is also a key element in the original model of *Neelin and Held* [1987], described above.

In the current analysis, we find that surface heat and moisture fluxes local to an atmospheric column do not correlate well with the characteristics of the convection in the column. This is probably because local fluxes contribute only weakly to vertically integrated budgets on the time scale of convective cells. The observed impact of these fluxes must therefore come from their cumulative effect on the thermodynamic profiles over long fetches [*Raymond*, 1995; *Emanuel*, 1995].

Though not strictly an atmospheric parameter, the SST will be shown to have an effect on convection outside of its role in determining surface thermodynamic fluxes.

2.5 The question of causality

Convection interacts with its environment in multiple ways with many feedbacks that make the assignment of causality difficult. However, if the time scale for the evolution of a potentially predictive parameter that is correlated in some way with convection is significantly longer than the time scale of a convective cell, then that parameter may be considered to be at least a partial "cause" of convection.

Raymond et al. [2015] indicated that the instability index may fall into this category, at least at higher latitudes or in tropical storms, where rotational effects rapidly neutralize unbalanced temperature perturbations induced directly by convective flows. In this case, the temperature pattern, and hence the pattern of instability index, is on the average in thermal wind balance with the vorticity pattern and evolves with changes in the absolute vorticity field. The vorticity evolves on the time scale of the inverse of the horizontal divergence, whereas the relaxation to balance occurs on the time scale of the inverse of absolute vorticity. Thus, the flow remains close to balance if the absolute vorticity is much greater in magnitude than the divergence. In this case, the instability index is governed by the vorticity pattern, and therefore evolves on a time scale longer than that of the convection itself. The instability index can therefore be said to partially "control" the convection on convective time scales. This mechanism clearly prevails in tropical cyclones [*Gjorgjievska and Raymond*, 2014; *Raymond et al.*, 2014; *Raymond and Kilroy*, 2019].

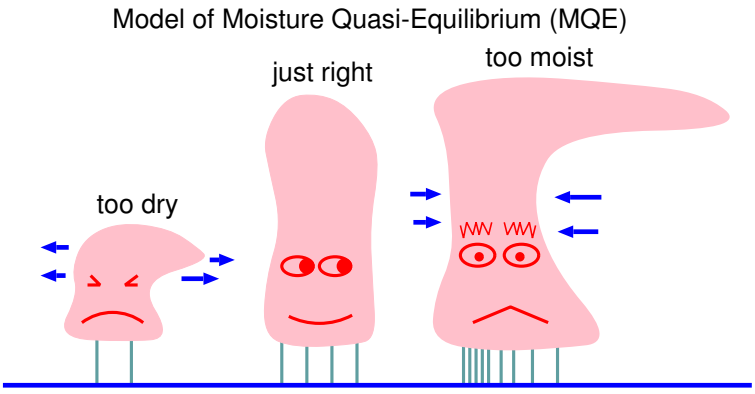

Figure 2. Illustration of moisture quasi-equilibrium. The cloud on the left dissipates due to excessive buoyancy loss from evaporation of condensate, moistening the atmosphere. The cloud on the right's buoyancy is less constrained by evaporation and produces excessive rain, which dries the atmosphere. In both, the atmosphere is driven toward the intermediate case, where the humidity is "just right". The blue arrows indicate the flow of moisture to or from the environment in the respective clouds.

Even at low latitudes where the Coriolis parameter is small, a temperature anomaly will tend to disperse over large areas due to the action of gravity waves. However, unlike the situation at higher latitudes, where the absolute vorticity provides an upper bound on the relaxation time for this process, the relaxation time increases in inverse proportion to the vertical scale of the temperature anomaly when the absolute vorticity is zero and the "relax to balance" process of higher latitudes becomes more complex near the equator.

Raymond et al. [2011], *Gjorgjievska and Raymond* [2014], and *Raymond et al.* [2014] showed that an inverse relationship exists between instability index and saturation fraction in tropical cyclone precursors. This "moisture quasi-equilibrium" (MQE) was reproduced in a cloud-resolving model using the weak temperature gradient approximation [*Raymond and Flores*, 2016] and in a high resolution model of tropical cyclogenesis [*Raymond and Kilroy*, 2019]. The reason for this correlation was revealed by *Singh and O'Gorman* [2013], who found that it results from the observed tendency of tropical oceanic updrafts to exist in a state of near-zero buoyancy. This leads to the inverse relationship between low to mid-tropospheric moisture and CAPE, or more accurately, the lower tropospheric version of CAPE [*Kuang*, 2008]. As noted above, the latter quantity is closely related to instability index.

Figure 2 helps clarify this phenomenon. If the environment is too dry, as on the left, a convective cell fails due to the mixing of dry air into the updraft, which evaporates condensate resulting in negative buoyancy. Such "sacrificial convection" moistens the environment. On the other hand, if the environment is very moist, as on the right, mixing in environmental air has much less effect on the updraft, allowing positive buoyancy to be maintained. In this case, the cell continues to ascend, producing precipitation and drying of the environment. As cells continue to form, the environmental humidity moves toward a critical value at which point convective entrainment produces nearly neutral buoyancy and MQE prevails, as in the center of figure 2. The equilibrium state is moist for weak convective instability and dry for strong instability, explaining the inverse relationship between instability (or instability index) and moisture (or saturation fraction).

As *Raymond* [2000] showed, movement toward moisture quasi-equilibrium is very rapid for strong convection, but very slow for weak convection. In the latter case, MQE is typically not reached and the actual saturation fraction is then less than the equilibrium value. In other words, in the weak convective case moisture quasi-equilibrium becomes an inequality. However, for strong convection, the saturation fraction is closely correlated with the instability index.

Physically, convective inhibition should be a powerful mechanism for suppressing convection, particularly over tropical oceans where the strong forcing that can occur over land is missing. In the absence of other mechanisms, boundary layer depletion by convective downdrafts with a corresponding increase in inhibition, followed by regeneration of the boundary layer by surface heat fluxes and a decrease in convective inhibition has long been known to be an effective control on convection [*Zipser*, 1969]. *Raymond* [1995] and *Emanuel* [1995] quantified this process.

Thayer-Calder and Randall [2015] found in numerical modeling that the subcloud layer's moist entropy was controlled more by dry entrainment than by convective downdrafts, suggesting that consideration the entropy budget in a deeper layer would be more appropriate. Independent evidence [*Kingsmill and Houze*, 1999; *Raymond et al.*, 2003; *Raymond et al.*, 2006] supports the idea that deep convective updrafts are supplied by a significantly deeper layer, which led to the above definition of DCIN.

The cycling of boundary layer entropy associated with downdrafts and surface fluxes adds a strong random element to the formation and decay of convection. However, the above-mentioned boundary layer models driven by SST gradients have the potential to impose some order on this randomness. A key assumption of these models is that the pressure distribution above the boundary layer is horizontally uniform, so that the pressure in the boundary layer is governed hydrostatically by the temperature there, and hence the temperature of the sea surface. Simple balance models can approximately predict the distribution of boundary layer winds and the associated convergence. However, as *Raymond et al.* [2006] showed, this assumption is sometimes violated to an extent that it produces boundary layer flows which differ significantly from the flows predicted by the simple theory.

3 Data and methods

Dropsonde data were used from OTREC [*UCAR et al.*, 2019] and PREDICT (`https://doi.org/10.5065/D6R78CD4`). Both projects deployed grids of dropsondes over tropical oceans from high altitude ($\approx$ 13 km) with spacings of order 1° in latitude and longitude in OTREC and 1.5° to 2° in PREDICT. Since the dropsonde spacing in PREDICT was slightly greater than in OTREC, the results from the former are somewhat more smoothed than for the latter.

The projects differed in their study regions and target selection algorithms. OTREC covered the East Pacific in an ITCZ-crossing pattern southwest of Costa Rica, the Colombian Pacific coastal region, and the far SW Caribbean in fixed patterns that were repeated at random intervals in order to avoid selection bias [*Fuchs-Stone et al.*, 2020]. PREDICT sought out regions in the Caribbean and Western Atlantic with pre-existing vorticity patches that were thought to have potential to grow into tropical cyclones.

The dropsonde data were ingested by the three-dimensional variational analysis scheme (3DVar) of *López-Carrillo and Raymond* [2011] to produce 0.25°×0.25° cartesian grids over a convex polygon covering the region in which dropsondes were deployed. No background fields from global analyses were ingested in order to avoid incorporating possibly spurious analysis results. As a consequence, fields outside of the polygon were set to a bad data value. The vertical domain of the analysis stretches from the surface to 16 km with a 200 m vertical resolution.

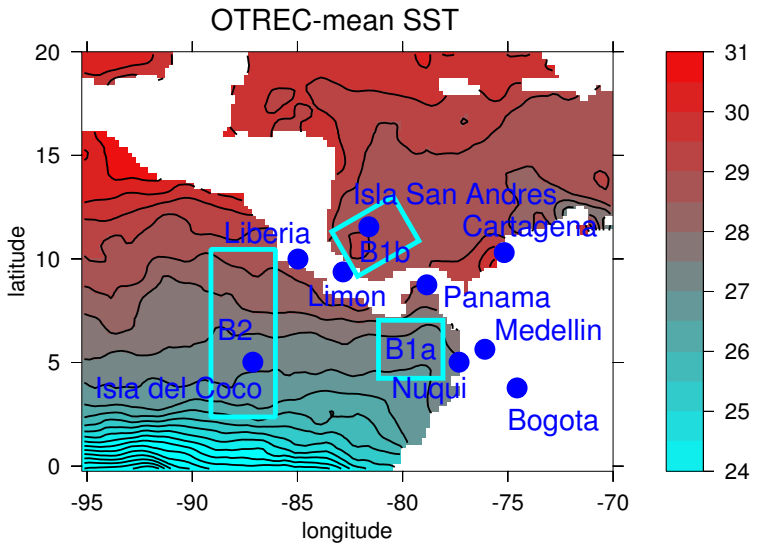

Figure 3. Map of the OTREC operational area along with the NOAA AVHRR SST averaged over the project period. The blue boxes represent the regions in which dropsondes were deployed.

The 3DVar scheme minimizes a cost function with various terms. Scalar analyses include terms forcing adherence to actual dropsonde values plus sufficient horizontal smoothing to make smooth interpolations between dropsondes. Smoothing in the vertical is minimal. Wind analyses contain similar terms plus strong adherence to mass continuity and zero vertical wind at the surface and 16 km. Vertical winds and mass fluxes result from this application of mass continuity. Actual analysis values above 13 km are not trustworthy since dropsonde data only exist below this elevation.

Unlike previous uses of this 3DVar scheme [*Raymond and López-Carrillo*, 2011; *Raymond et al.*, 2011; *Gjorgjievska and Raymond*, 2014; *Juračić and Raymond*, 2016], individual $0.25°\times0.25°$ columns were analyzed and the results composited in various ways. This avoids the selection bias inherent in earlier applications of the method in which averages over selected regions were used. Defining the boundaries of "interesting" regions is always a point of contention.

Figure 3 shows the OTREC operational area and the three boxes in which dropsondes were deployed. Boxes B1a and B1b were combined into a single box consisting of B1a extended to the north across Panama and into the Caribbean late in the project. Also shown is the daily NOAA/PSL AVHRR SST (`https://www.ncei.noaa.gov/data/sea-surface-temperature-optimum-interpolation/access/avhrr-only/`) averaged over the period of the project. Data from all 22 missions were incorporated into our analysis. (One special mission in conjunction with a NOAA Hurricane Research Division flight deployed sondes near $(-92°, 11°)$. Data from this mission are included in our analysis.)

Figure 4 shows a similar map for the area covered by the PREDICT project. Twenty-three of the 26 PREDICT missions with the G-V were used (RF01, RF21, RF23 omitted), though some missions had higher quality dropsonde grids than others. The 3 omitted missions had either very poor dropsonde grids or bad data. As in figure 3, an average of the AVHRR SST was taken over the project period. Note that SST gradients were much weaker in the PREDICT region than in OTREC. The yellow dots, which show a randomly selected sample of the $0.25°\times0.25°$ columns used in the analysis, are presented to give a sense of the areas covered.

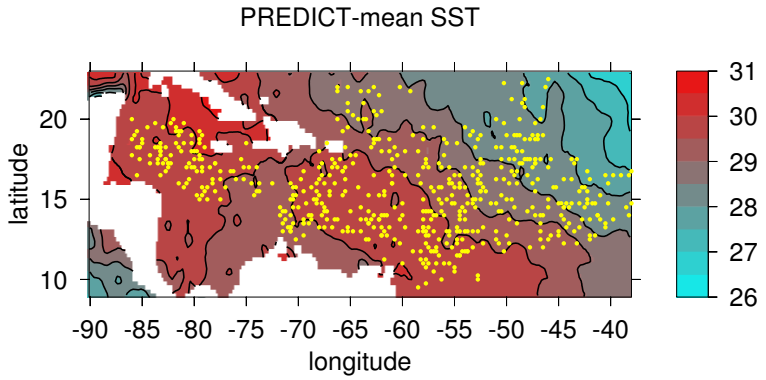

Figure 4. Map of the PREDICT operational area along with the NOAA AVHRR SST averaged over the project period. The yellow dots indicate the area covered by the 23 selected PREDICT missions.

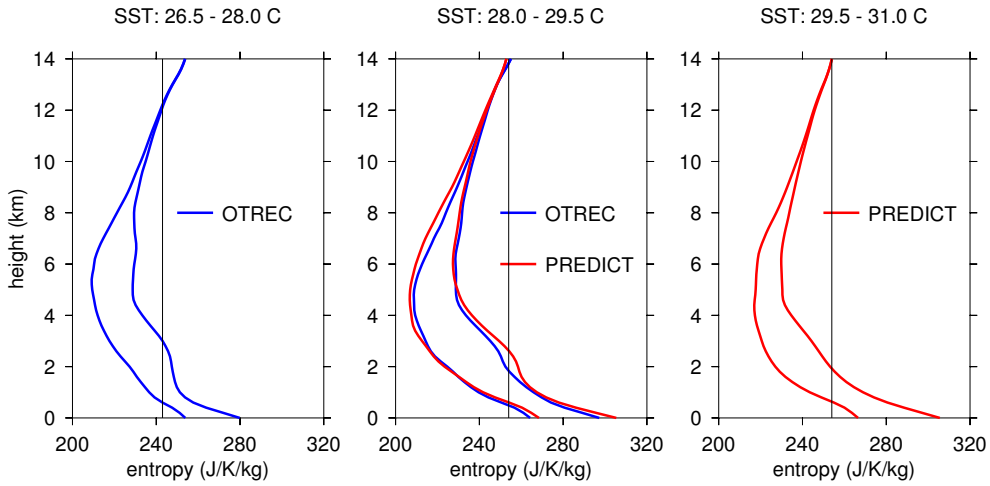

Figure 5. Mean entropy soundings sorted by SST from PREDICT (red) and OTREC (blue). Overlap between SSTs between the two projects occurred mainly in the range 28-29.5 C. In each sounding the left curve is the moist entropy and the right curve is the saturated moist entropy. The thin black lines indicate the moist entropy of a parcel with entropy equal to the average in the 0-1 km layer.

4 Results

4.1 Environmental conditions

We first examine the mean temperature and moisture profiles in the two projects, sorted into three SST ranges in figure 5. Soundings in the 28-29.5 C range are very similar in the OTREC and PREDICT cases. The temperature soundings above 4 km (as represented by the saturated moist entropy) are similar for all SST ranges as well. However, there are differences in relative humidity over the three ranges (as represented by the difference between entropy and saturated moist entropy curves), with moister air occurring in the 29.5-31 C range. The main differences occur below 4 km, with an inversion in the 1-3 km range that decreases with increasing SST. The surface values of moist and saturated moist entropy in the 26.5-28 C range are significantly less than those oc-

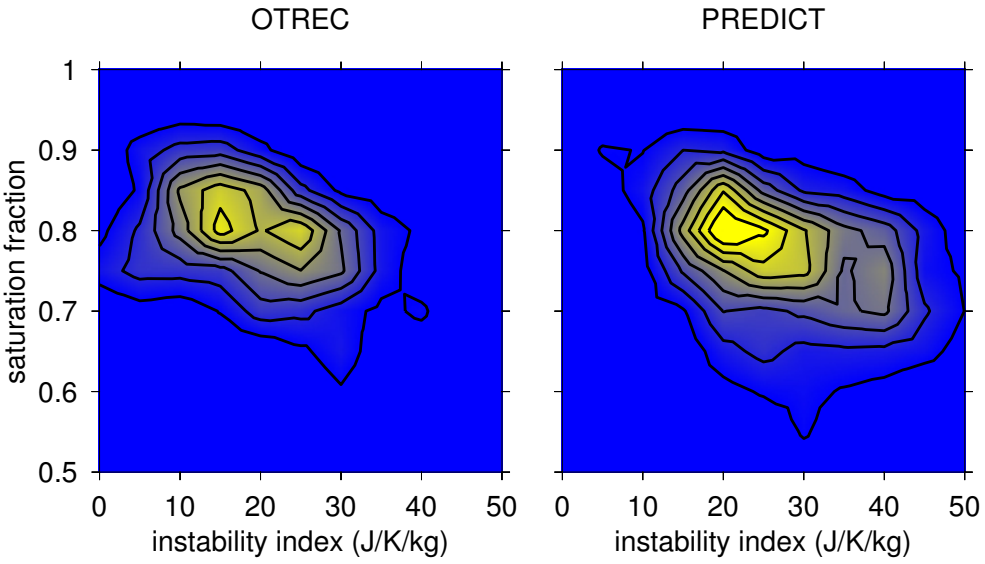

Figure 6. Frequency of occurrence of saturation fraction-instability index pairs for the OTREC (left) and PREDICT (right) cases. Yellow regions have the highest frequency of occurrence while blue regions have the lowest. Frequency is not normalized so the contour interval is not meaningful.

curring at higher SSTs and the low to mid-tropospheric relative humidity is lower in the 28-29.5 C range than in the other SST ranges.

Figure 6 shows the frequency of occurrence of saturation fraction-instability index pairs for OTREC and PREDICT. This figure shows that the inverse relationship between the two variables characteristic of MQE holds for both the OTREC and PREDICT cases. It also shows that the most common values of saturation fraction in both cases are in the range 0.7-0.9. Ranges for instability index in the two cases differ somewhat, with 5-30 J K^{-1} kg^{-1} being common for OTREC and 10-40 J K^{-1} kg^{-1} for PREDICT.

Previous work on tropical cyclone precursors [*Raymond et al.*, 2011; *Gjorgjievska and Raymond*, 2014; *Raymond et al.*, 2014] found an inverse correlation between mid-level vorticity and instability index. This results from relaxation of the temperature field to a balanced thermal wind state in a pre-cyclone mid-level vortex [*Raymond*, 2012], which produces a warm anomaly above the vortex and a cool anomaly below. This combination reduces the instability index. Figure 7 shows the frequency of occurrence of instability index vs. 3-5 km relative vorticity for OTREC and PREDICT. The inverse correlation between vorticity and instability index is clearly visible in the PREDICT case, with larger values of the vorticity associated with smaller values of the instability index. However, the correlation is absent from the OTREC data. Recall that PREDICT focused on tropical cyclone precursors, which may explain why there are larger vorticity values for this case.

4.2 Moisture convergence, entropy divergence, and mass fluxes

We now examine how the vertically integrated moisture convergence relates to the four atmospheric parameters discussed in section 2.4, instability index, saturation fraction, surface thermodynamic fluxes, and deep convective inhibition, plus the SST. Moisture convergence is highly correlated with precipitation as (5) indicates.

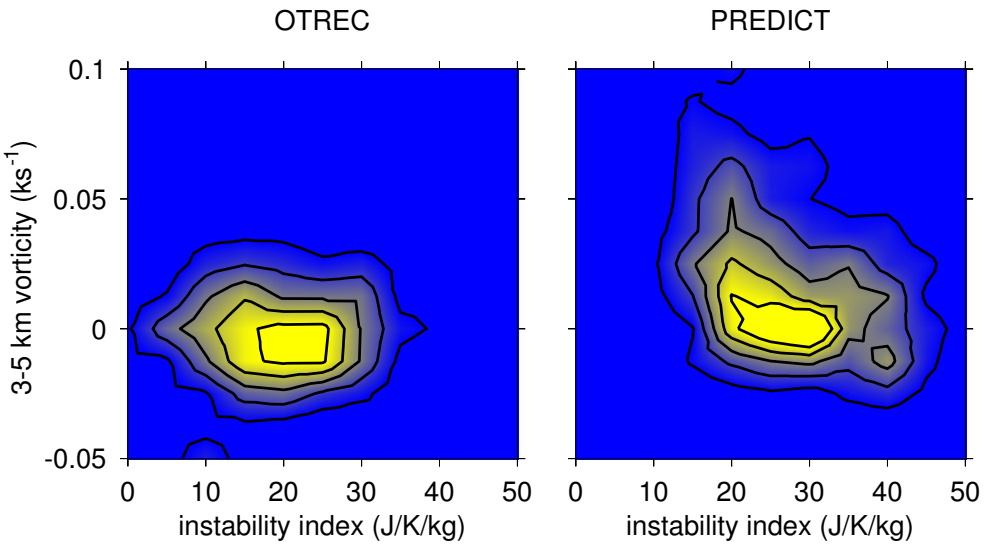

Figure 7. As in figure 6 except for 3-5 km relative vorticity-instability index pairs.

Moisture convergence	OTREC	PREDICT
II	0.077	0.116
SF	0.144	0.065
DCIN	0.108	0.041
EFLUX	0.007	0.018
SST	0.007	0.009
CAPE	0.002	0.012

Table 1. Fraction of variance explained in regressions of moisture convergence against instability index (II), saturation fraction (SF), deep convective inhibition (DCIN), surface moist entropy flux (EFLUX), sea surface temperature (SST), and convective available potential energy (CAPE).

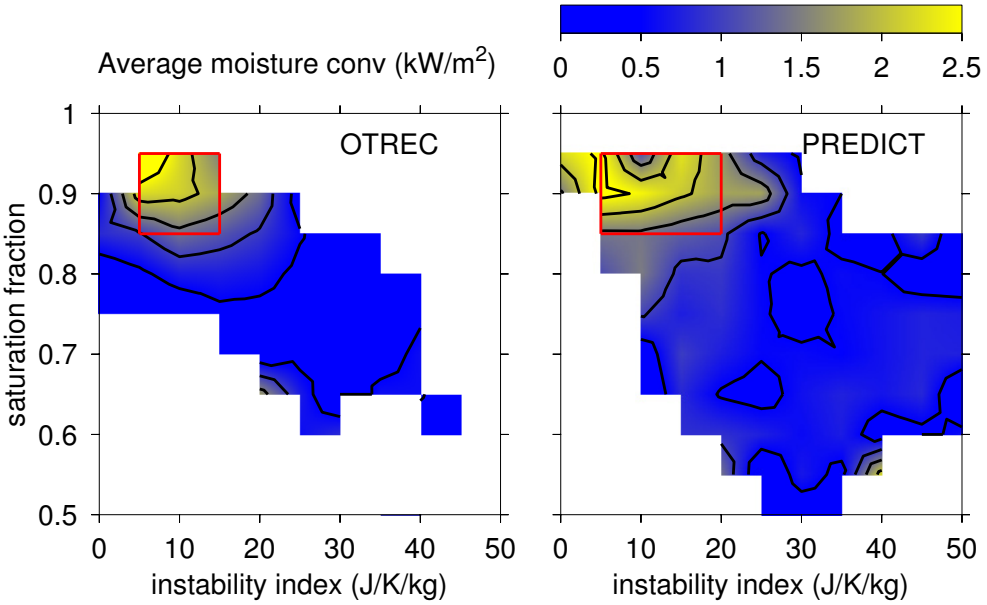

Figure 8. Average moisture convergence as a function of instability index and saturation fraction for OTREC (left) and PREDICT (right). The red boxes indicate areas of strongest moisture convergence. The contour interval is 0.5 kW m^{-2}.

As a preliminary filter to determine which of these parameters to consider further, table 1 shows the fraction of variance explained in regressions of the moisture convergence onto each parameter. Only instability index, saturation fraction, and deep convective inhibition exhibit fractions exceeding 10% for one project or the other. The surface moist entropy flux and the SST show 2% or less of explained variance, so the effects of these two parameters on moisture convergence are neglected.

The fractions explained by the three surviving variables differ markedly between OTREC and PREDICT. For OTREC, saturation fraction exhibits the strongest correlation, while instability index dominates for PREDICT. Deep convective inhibition is more important than instability index for OTREC, while the reverse is true for PREDICT.

It is noteworthy that the fractions of variance explained by all three parameters are small, indicating either that unexplored variables exist or that the chaotic behavior of convection plays a large role in the variance of moisture convergence. Since each 0.25°× 0.25° column is treated independently of the others, correlation effects between columns are not considered, which may be an additional factor in reducing the fraction of variance explained. However, similar calculations on real world data averaged over convective disturbances lead to similar results [*Raymond and Flores*, 2016]. The values of explained variance are robust to subsetting the data in the two projects, so the differences seen between OTREC and PREDICT are likely to be real.

Figure 8 shows the average over each project of positive-only moisture convergence for OTREC and PREDICT as a function of instability index and saturation fraction. In both cases the largest average moisture convergence occurs for very high values of saturation fraction (≈ 0.9) and low values of instability index (5-15 J K^{-1} kg^{-1} for OTREC and 5-20 J K^{-1} kg^{-1} for PREDICT). For comparison purposes, 2 kW m^{-2} is equivalent to about 70 mm day^{-1} of precipitation.

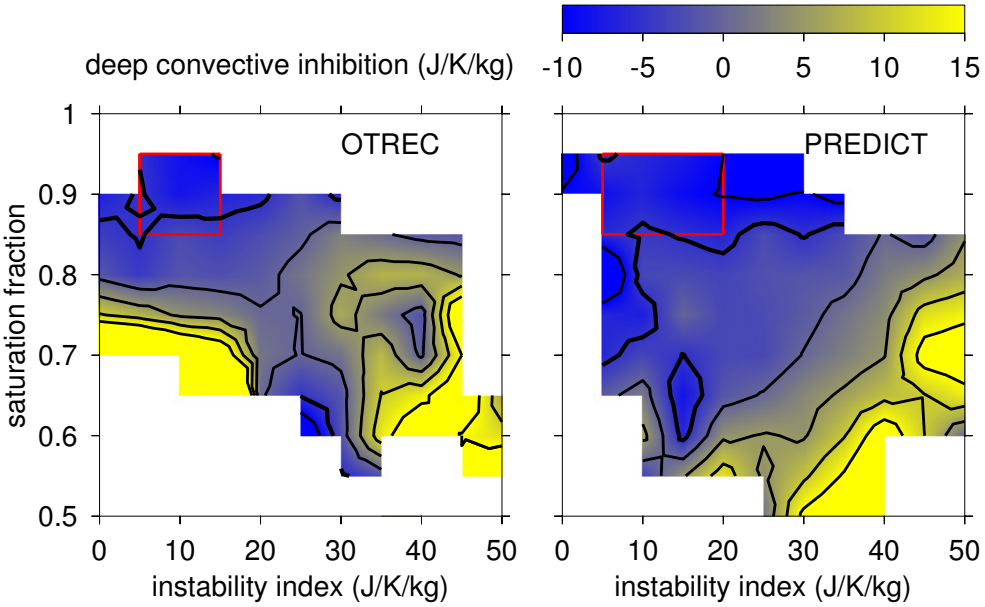

Figure 9. Average value of deep convective inhibition as a function of instability index and saturation fraction for OTREC (left) and PREDICT (right). The contour interval is 5 J K^{-1} kg^{-1} and the heavy contour is -5 J K^{-1} kg^{-1}. The red boxes show regions of large moisture convergence as in figure 8.

Entropy divergence	OTREC	PREDICT
II	0.012	0.039
SF	0.001	0.001
DCIN	0.084	0.020
EFLUX	0.048	0.011
SST	0.025	0.000
CAPE	0.008	0.000

Table 2. As in table 1 except fraction of explained variance for entropy divergence.

Figure 9 shows the average value of deep convective inhibition as a function of instability index and saturation fraction. Values of DCIN < 5 J K^{-1} kg^{-1} are widespread. DCIN < -5 J K^{-1} kg^{-1} is mostly limited to the regions of large average moisture convergence for OTREC, as illustrated in figure 8. However, these low DCIN values are distributed somewhat more broadly in PREDICT.

Table 2 shows the fraction of variance explained for the entropy divergence regressed against the same set of variables used in table 1. Generally, these variables explain a smaller fraction of the variance in entropy divergence than in moisture convergence. In particular, instability index and saturation fraction, which play an important role in the variance of moisture convergence, exhibit almost no correlation with entropy divergence. Only deep convective inhibition explains more than 5% and only in OTREC.

The mass flux profile of deep convection is related to both the moisture convergence and the entropy divergence. We characterize the vertical mass flux profile by average values in the 3-5 km and 7-9 km layers, MFLUXLO and MFLUXHI, and define the differ-

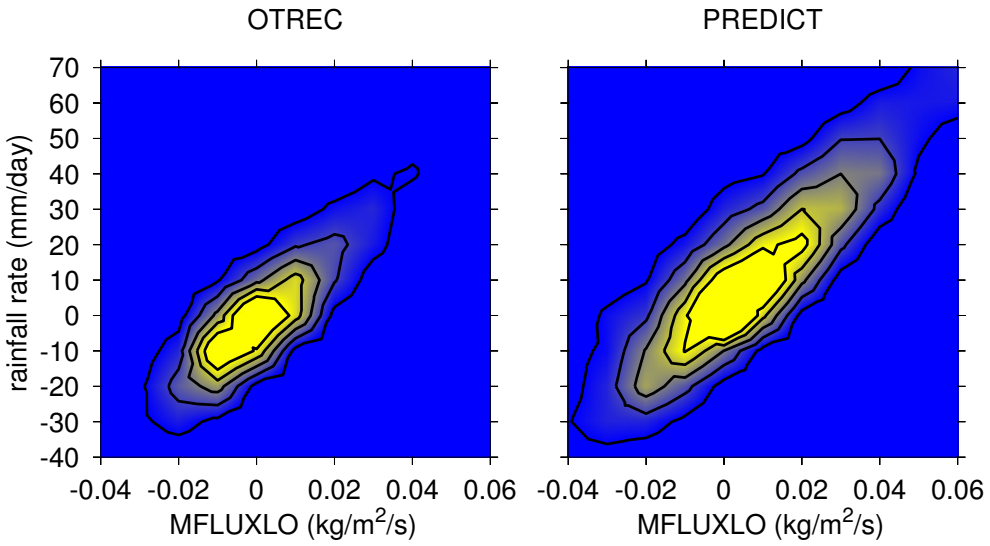

Figure 10. As in figure 6 except MFLUXLO-rainfall rate pairs. Negative rainfall rates are unphysical and result from uncompensated subsidence and drying.

ence between these mass fluxes by

$$\text{MFLUXDIF} = \text{MFLUXHI - MFLUXLO.} \tag{18}$$

Positive values of MFLUXDIF thus correspond to top-heavy mass flux profiles while negative values represent bottom-heavy profiles.

Figure 10 plots the rainfall rate for OTREC and PREDICT, computed using (9), vs. MFLUXLO, showing that the two are closely correlated in both cases. This is expected since the vertical mass flux is driven by the latent heat release associated with precipitation. In these calculations, radiative heating is arbitrarily set to -200 W m^{-2}. It is noteworthy that maximum rainfall rates in PREDICT are significantly greater than in OTREC. This most likely reflects the inclusion of measurements from intensifying tropical cyclone precursors in PREDICT.

Based on limited data (including case studies from PREDICT), *Raymond et al.* [2015] found that the upper bound on MFLUXDIF exhibits a strong dependence on SST. The left panel of figure 11, which combines data from OTREC and PREDICT, provides additional support for this hypothesis. For SST = 26 C, MFLUXDIF ≤ 0.01 kg m^{-2} s^{-1}, while for SST = 30 C, MFLUXDIF ≤ 0.06 kg m^{-2} s^{-1}.

Arguments made by *Back and Bretherton* [2006], *Raymond et al.* [2009], *Inoue and Back* [2015], and others suggest that moist static energy (or moist entropy) divergence should be positive for top-heavy convective mass flux profiles and negative for bottom-heavy profiles and therefore should present a similar picture when plotted against SST. The right panel of figure 11 verifies this. Thus, low SSTs result in bottom-heavy mass fluxes and entropy convergence, while high SSTs allow but do not guarantee top-heavy profiles and entropy divergence.

The reason for the broad ranges of MFLUXDIF and entropy divergence seen in figure 11 for high SSTs as well as the small fractions of explained variance in table 2 may lie with the work of *Masunaga and L'Ecuyer* [2014], *Inoue and Back* [2015] and *Inoue and Back* [2017]. As explained in section 2.2, they find that convective systems over warm tropical oceans undergo a life cycle of initial entropy (or moist static energy) convergence

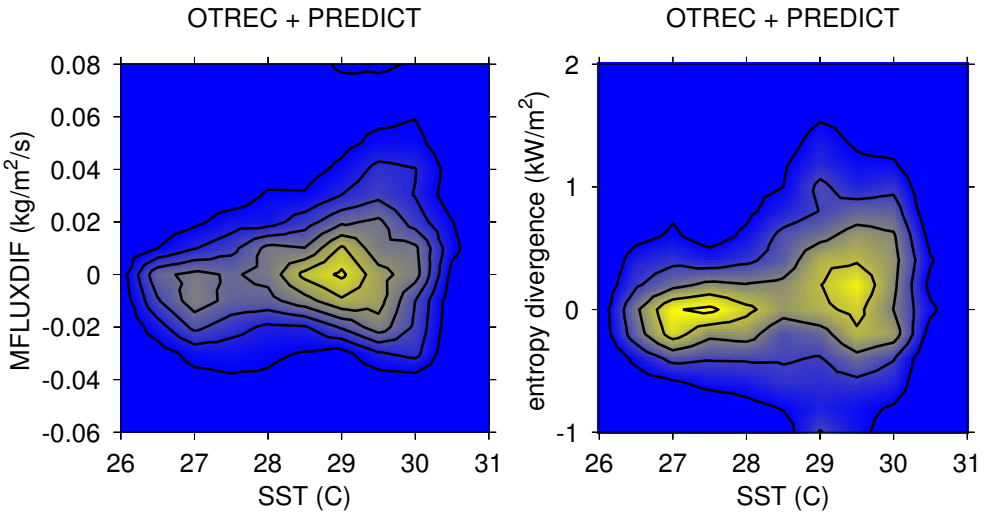

Figure 11. As in figure 6 except for MFLUXDIF-SST (left) and entropy divergence-SST (right) pairs for the combined OTREC and PREDICT data sets.

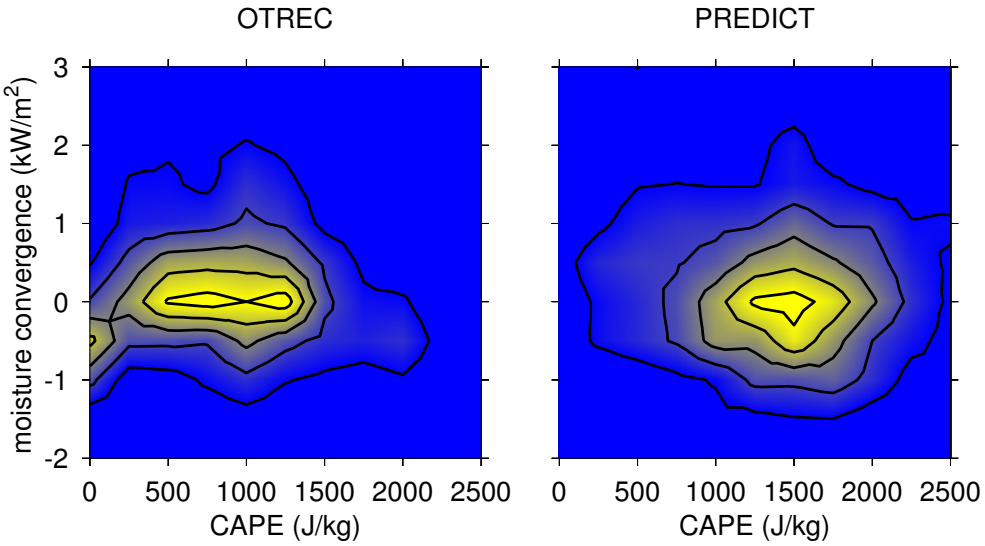

Figure 12. As in figure 6 except for CAPE-moisture convergence pairs.

followed by entropy divergence during decay. Thus, a broad distribution of entropy divergence (and MFLUXDIF) is to be expected for high SST.

4.3 Convective available potential energy

Tables 1 and 2 show that the fractions of variance in moisture convergence and entropy divergence explained by CAPE are negligible for both OTREC and PREDICT. This point is reinforced by the frequency of occurrence plot of CAPE-moisture convergence pairs shown in figure 12; there is no discernible relationship between the two as long as CAPE is positive. Similar null results hold for entropy divergence (not shown). There is a correlation between CAPE and SST for OTREC (not shown), which is to be expected, given the strong latitudinal gradient in boundary layer moist entropy associated with the SST gradient. Such a correlation does not occur for PREDICT, because

the very low SSTs of the East Pacific equatorial region do not exist in the PREDICT domain.

4.4 Differences between OTREC and PREDICT convection

Differences in convection between OTREC and PREDICT are likely to arise from two sources, the stronger vorticity and the generally higher SSTs in PREDICT. Larger vorticity alters the relationship between heating and warming, and thus the development of temperature anomalies that are responsible for changes in the instability index. This is likely to alter the feedback between evaporation of stratiform precipitation and the effect on subsequent convection. Deep convective inhibition is likely more important in OTREC due to the lower SSTs and stronger SST gradients in comparison with PREDICT.

However, OTREC and PREDICT share many characteristics. In particular, convection in both areas appears to be sensitive to values of saturation fraction and instability index, with the strongest convection occurring for large saturation fraction and small instability index. The inverse relationship between these two parameters exists in both regions. Deep convective inhibition is important in both cases, though more so in OTREC. In both OTREC and PREDICT, local surface moisture and moist entropy fluxes appear to have little direct influence. The well-documented effects of these fluxes on convection in many situations are therefore likely to be non-local, manifesting themselves via modification of thermodynamic profiles by surface fluxes over an extended fetch. Finally, CAPE is related neither to moisture convergence nor entropy divergence in either project.

5 Lessons for cumulus parameterization

The above results impose certain constraints on convective parameterizations. The inclusion of data from both OTREC and PREDICT, with their very different regimes, suggests broad applicability of these results to tropical oceans. Some elements in the following list are already well known, others less so.

1. It is well established that mean precipitation increases rapidly with increasing saturation fraction above values of ≈ 0.7 [*Bretherton et al.*, 2004; *Neelin et al.*, 2009; *Kim and Co-Authors*, 2014]. This behavior is reproduced in our observations. However, the ability of parameterizations to reproduce this sensitivity is not a given, as shown by *Derbyshire et al.* [2004].
2. Less well known is the strong sensitivity of rainfall to the low to mid-tropospheric moist convective instability, represented here by the instability index. The factors controlling instability index in OTREC and PREDICT are likely to differ somewhat due to the generally weak vorticity at low latitudes. However, the effect of instability index on convection is similar between the two regions, namely, small but positive values of instability index result in the heaviest average precipitation.
3. Saturation fraction and instability index are broadly anti-correlated, with small instability index being associated with large saturation fraction. We call this relationship "moisture quasi-equilibrium" (MQE) and it is enforced by the behavior of convection, which drives the saturation fraction toward a set point which is larger for smaller instability index. In weak convective cases the adjustment time for saturation fraction is large and actual saturation fraction values are often smaller than the set point. This behavior should be reproduced by cumulus parameterizations.
4. It is perhaps no surprise that convective inhibition is a significant control parameter for deep convection. However, evaluating the buoyancy of a parcel with properties averaged over a rather deep layer is important in its calculation, since observations suggest that deep convective updrafts draw on air from well above the

subcloud layer. We define the "deep convective inhibition" (DCIN) with this caveat in mind.

5. CAPE is often used to trigger convection in cumulus parameterizations. Tables 1 and 2 as well as figure 12 strongly suggest that CAPE is not an appropriate trigger for convection in such parameterizations, except possibly as a threshold indicator for conditional instability. However, a combination of positive instability index and negative deep convective inhibition may serve equally well in this role.
6. Given the apparent importance of surface heat and moisture fluxes seen in numerous studies in the generation of deep convection, it may be surprising that the effect of local surface fluxes on convection is generally small. However, this apparent paradox is likely resolved by the realization that the effects of surface fluxes are only manifested by the accumulated changes they make in the temperature and humidity soundings, which are significant only over long fetches.
7. Rainfall is tightly correlated with the 3-5 km vertical mass flux. This is no surprise given that most atmospheric moisture is concentrated in the lowest few kilometers. More interesting is the effect of high SST on the production of top-heavy vertical mass flux profiles and entropy divergence. This doesn't always occur, but may be limited to late in the life cycle of convective systems in high-SST environments.
8. All of the above results come from averaging over broad probability distributions. The breadth of these distributions may simply indicate that we have insufficient data to narrow them, or that we haven't yet extracted all of the relevant control parameters. However, it is also possible that their breadth simply reflects the chaotic nature of atmospheric convection. Whatever the cause, this suggests the importance of implementing stochastic variability in the construction of cumulus parameterizations.

6 Conclusions

This paper uses gridded dropsonde analyses from two field programs over tropical oceans, Organization of Tropical East Pacific Convection (OTREC2019) and Pre-Depression Investigation of Cloud-Systems in the Tropics (PREDICT2010) to characterize those factors in tropical oceanic convection pertinent to convective parameterizations. OTREC studied ITCZ convection in the near-equatorial waters of the far East Pacific and Southwest Caribbean while PREDICT focused on convection in convective clusters over the tropical Atlantic and Caribbean that were judged to be candidates for tropical cyclogenesis. PREDICT thus studied regions with higher SSTs and larger values of planetary and relative vorticity than OTREC.

We have purposely avoided filtering our results through the lens of existing theoretical models of convection, e.g., plumes, thermals, stratiform vs. convective rain, cold pools, etc. In this way we strive to extract the "emergent properties" of convection on the mesoscale as observed in the real world.

The effect of various thermodynamic parameters on factors important to cumulus parameterizations are studied. These include the saturation fraction (a kind of column relative humidity), the instability index (a measure of low to mid-tropospheric moist convective instability), the deep convective inhibition (a convective inhibition index focused on the lifting of parcels from a deep layer adjacent to the surface), and the SST. Local surface heat and moisture fluxes have little direct effect. All of these parameters can be derived from explicitly computed fields in large-scale models.

The main results arising from this study are that the strongest moisture convergence, and hence the heaviest mean precipitation, occur for large values of saturation fraction and small values of both instability index and deep convective inhibition. The main effect of high sea surface temperatures is to increase the probability of convection

with strong entropy divergence and top-heavy mass flux profiles. These results impose significant constraints on the allowable behavior of cumulus parameterizations.

As with most measurements of convective properties in the field, they come with a large overlay of "noise", which represents some combination of insufficient data, incomplete understanding (e.g., the role of wind shear), and the natural variability of convection. For this reason, most results are expressed in terms of probability distributions, which facilitate the computation of not only mean values but also distribution widths, which may be useful in the calibration of stochastic cumulus parameterizations.

Notable for its lack of effect on moisture convergence and entropy divergence is the CAPE. It follows that the widespread use of CAPE as a convective trigger in cumulus parameterizations needs to be reconsidered.

Acknowledgments

We thank the Earth Observing Laboratory of the National Center for Atmospheric Research for their excellent support in both OTREC and PREDICT. The professional operation of the Gulfstream V aircraft and the related observational tools deserve particular mention, as does the handling of the resulting data. The support and guidance of Eric DeWeaver of the National Science Foundation for OTREC is highly appreciated. The NCAR/EOL AVAPS Dropsonde QC Data DOI `https://doi.org/10.26023/EHRT-TN96-9W04`. Data are provided by NCAR/EOL under the sponsorship of the National Science Foundation `https://data.eol.ucar.edu/`. This work was supported by National Science Foundation Grant No. 1758513.

7 References

Adames, A. F. and D. Kim (2016). The MJO as a dispersive, convectively coupled moisture wave. *J. Atmos. Sci.*, *73*, 913-941.

Arakawa, A. (2004). The cumulus parameterization problem. *J. Climate*, *17*, 2493-2525.

Arakawa, A. and W. H. Schubert (1974). Interaction of a cumulus cloud ensemble with the large-scale environment, Part I. *J. Atmos. Sci.*, *31*, 674-701.

Araligidad, N. M. and E. D. Maloney (2008). Wind-driven latent heat flux and the intraseasonal oscillation. *Geophys. Res. Lett.*, *35*, L04815, doi:10.1029/2007GL032746.

Back, L, E. and C. S. Bretherton (2006). Geographic variability in the export of moist static energy and vertical motion profiles in the tropical Pacific. *Geophys. Res. Lett.*, *33*, L17810, doi:10.1029/2006GL026672.

Back, L. E. and C. S. Bretherton (2009). On the relationship between SST gradients, boundary layer winds, and convergence over the tropical oceans. *J. Climate*, *22*, 4182-4196.

Battisti, D. S., E. S. Sarachik and A. C. Hirst (1999). A consistent model for the large-scale steady surface atmospheric circulation in the tropics. *J. Climate*, *12*, 2956-2964.

Benedict, J. J. and D. A. Randall (2009). Structure of the Madden-Julian oscillation in the superparameterized CAM. *J. Atmos. Sci.*, *66*, 3277-3296.

Betts, A. K. (1986). A new convective adjustment scheme, Part I. *Quart. J. Roy. Meteor. Soc.*, *112*, 677-691.

Betts, A. K. and M. J. Miller (1986). A new convective adjustment scheme, Part II. *Quart. J. Roy. Meteor. Soc.*, *112*, 693-709.

Betts, A. K. and M. J. Miller (1993). The Betts-Miller scheme. *The Representation of Cumulus Convection in Numerical Models, K. A. Emanuel and D. J. Raymond Eds, American Meteorological Society*, 107-121.

Braun, S. A., P. A. Newman and G. M. Heymsfield (2016). NASA's hurricane and severe storm sentinel (HS3) investigation. *Bull. Am. Meteor. Soc.*, *97*, 2085-2102.

Bretherton, C. S., M. E. Peters and L. E. Back (2004). Relationships between water vapor path and precipitation over the tropical oceans. *J. Climate*, *17*, 1517-1528.

Bretherton, C. S. and P. K. Smolarkiewicz (1989). Gravity waves, compensating subsidence and detrainment around cumulus clouds. *J. Atmos. Sci.*, *46*, 740-759.

Cheng, M.-D. and A. Arakawa (1997). Inclusion of rainwater budget and convective downdrafts in the Arakawa-Schubert cumulus parameterization. *J. Atmos. Sci.*, *54*, 1359-1378.

Churchill, D. D. and R. A. Houze Jr (1984). Development and structure of winter monsoon cloud clusters on 10 December 1978. *J. Atmos. Sci.*, *41*, 933-960.

Derbyshire, S. H., I. Beau, P. Bechtold, J.-Y. Grandpeix, J.-M. Piriou, J.-L. Redelsperger and P. M. M. Soares (2004). Sensitivity of moist convection to environmental humidity. *Quart. J. Roy. Meteor. Soc.*, *130*, 3055-3079.

Elsberry, R. L. and P. A. Harr (2008). Tropical cyclone structure (TCS08) field experiment science basis, observational platforms, and strategy. *Asia-Pacific Journal of Atmospheric Sciences*, *44*, 209-231.

Emanuel, K. A. (1986). An air-sea interaction theory for tropical cyclones. *J. Atmos. Sci.*, *43*, 585-604.

Emanuel, K. A. (1987). An air-sea interaction model of intraseasonal oscillations in the tropics. *J. Atmos. Sci.*, *44*, 2324-2340.

Emanuel, K. A. (1995). The behavior of a simple hurricane model using a convective scheme based on subcloud-layer entropy equilibrium. *J. Atmos. Sci.*, *52*, 3960-3968.

Fuchs-Stone, Ž., D. J. Raymond and S. Sentíc (2020). OTREC2019: Convection over the East Pacific and Southwest Caribbean. *Geophys. Res. Lett.*, *47*, doi:10.1029/2020GL087564.

Fuchs, Ž. and D. J. Raymond (2017). A simple model of intraseasonal oscillations. *J. Adv. Model. Earth Syst.*, *9*, doi:10.1002/2017MS000963.

Gjorgjievska, S. and D. J. Raymond (2014). Interaction between dynamics and thermodynamics during tropical cyclogenesis. *Atmos. Chem. Phys.*, *14*, 3065-3082.

Grabowski, W. W. (2001). Coupling cloud processes with the large-scale dynamics using the cloud-resolving convection parameterization (CRCP). *J. Atmos. Sci.*, *58*, 978-997.

Grabowski, W. W. (2003). MJO-like coherent structures. *J. Atmos. Sci.*, *60*, 847-864.

Hayashi, Y. and D. G. Golder (1997a). United mechanisms for the generation of low- and high-frequency tropical waves. Part I: Control experiments with moist convective adjustment. *J. Atmos. Sci.*, *54*, 1262-1276.

Hayashi, Y. and D. G. Golder (1997b). United mechanisms for the generation of low- and high-frequency tropical waves. Part II: Theoretical interpretations. *J. Meteor. Soc. Japan*, *75*, 775-797.

Houze, R. A. (1989). Observed structure of mesoscale convective systems and implications for large-scale heating. *Quart. J. Roy. Meteor. Soc.*, *115*, 425-461.

Houze, R. A. (1997). Stratiform precipitation in regions of convection. *Bull. Am. Meteor. Soc.*, *78*, 2179-2196.

Houze, R. A. (2004). Mesoscale convective systems. *Rev. Geophys.*, *42*, RG4003, doi:10.1029/2004RG000150.

Houze, R. A. and C. P. Cheng (1981). Inclusion of mesoscale updrafts and downdrafts in computations of vertical fluxes by ensembles of tropical clouds. *J. Atmos. Sci.*, *38*, 1751-1770.

Inoue, K. and L. E. Back (2015). Gross moist stability assessment during TOGA COARE. *J. Atmos. Sci.*, *72*, 4148-4166.

Inoue, K. and L. E. Back (2017). Gross moist stability analysis. *J. Atmos. Sci.*, *74*, 1819-1837.

Juračić, A. and D. J. Raymond (2016). The effects of moist entropy and moisture budgets on tropical cyclone development. *J. Geophys. Res.*, *121*, 9458-9473.

Khairoutdinov, M., D. Randall and C. DeMott (2005). Simulations of the atmospheric general circulation using a cloud-resolving model as a superparameterization of physical processes. *J. Atmos. Sci.*, *62*, 2136-2154.

Khairoutdinov, M. F. and D. A. Randall (2001). A cloud resolving model as a cloud parameterization in the NCAR community climate system model. *Geophys. Res. Lett.*, *28*, 3617-3620.

Khairoutdinov, M. F. and K. Emanuel (2018). Intraseasonal variability in a cloud-permitting near-global equatorial aquaplanet model. *J. Atmos. Sci.*, *75*, 4337-4355.

Kim, D. and Co-Authors (2014). Process-oriented MJO simulation diagnostic. *J. Climate*, *27*, 5379-5395.

Kingsmill, D. E. and R. A. Houze Jr (1999). Kinematic characteristics of air flowing into and out of precipitating convection over the west Pacific warm pool. *Quart. J. Roy. Meteor. Soc.*, *125*, 1165-1207.

Kuang, Z. (2008). Modeling the interaction between cumulus convection and linear gravity waves using a limited-domain cloud system-resolving model. *J. Atmos. Sci.*, *65*, 576-591.

Lindzen, R. S. and S. Nigam (1987). On the role of sea surface temperature gradients in forcing low-level winds and convergence in the tropics. *J. Atmos. Sci.*, *44*, 2418-2436.

López-Carrillo, C. and D. J. Raymond (2011). Retrieval of three-dimensional wind fields from Doppler radar data using an efficient two-step approach. *Atmos. Meas. Tech.*, *4*, 2717-2733.

Maloney, E. D. and S. K. Esbensen (2003). The amplification of east Pacific Madden-Julian oscillation convection and wind anomalies during June-November. *J. Climate*, *16*, 3482-3497.

Maloney, E. D. and S. K. Esbensen (2005). A modeling study of summertime east Pacific wind-induced ocean-atmosphere exchange in the intraseasonal oscillation. *J. Climate*, *18*, 568-584.

Maloney, E. D. and A. H. Sobel (2004). Surface fluxes and ocean coupling in the tropical intraseasonal oscillation. *J. Climate*, *17*, 4368-4386.

Manabe, S., J. Smagorinsky and R. F. Strickler (1965). Simulated climatology of a general circulation model with a hydrologic cycle. *Mon. Wea. Rev.*, *93*, 769-798.

Mapes, B. E. (1993). Gregarious tropical convection. *J. Atmos. Sci.*, *50*, 2026-2037.

Masunaga, H. and T. S. L'Ecuyer (2014). A mechanism of tropical convection inferred from observed variability in the moist static energy budget. *J. Atmos. Sci.*, *71*, 3747-3766.

Montgomery, M. T., C. Davis, T. Dunkerton, Z. Wang, C. Velden, R. Torn, S. J. Majumdar, F. Zhang, R. K. Smith, L. Bosart, M. M. Bell, J. S. Haase, A. Heymsfield, J. Jensen, T. Campos and M. A. Boothe (2012). The pre-depression investigation of cloud systems in the tropics (PREDICT) experiment. *Bull. Am. Meteor. Soc.*, *93*, 153-172.

Neelin, J. D., I. M. Held and K. H. Cook (1987). Evaporation-wind feedback and low-frequency variability in the tropical atmosphere. *J. Atmos. Sci.*, *44*, 2341-2348.

Neelin, J. D., O. Peters and K. Hales (2009). The transition to strong convection. *J. Atmos. Sci.*, *66*, 2367-2384.

Neelin, J. D. and I. M. Held (1987). Modeling tropical convergence based on the moist static energy budget. *Mon. Wea. Rev.*, *115*, 3-12.

Ramage, C. S. (1971). Monsoon meteorology. *Academic Press, New York*, 296 pp.

Rasp, S., M. S. Pritchard and P. Gentine (2018). Deep learning to represent subgrid processes in climate models. *Proceedings of the National Academy of Science*, *115 (39)*, 9684-9689, doi:10.1073/pnas.1810286115.

Raymond, D. J. (1995). Regulation of moist convection over the west Pacific warm pool. *J. Atmos. Sci.*, *52*, 3945-3959.

Raymond, D. J. (2000). Thermodynamic control of tropical rainfall. *Quart. J. Roy. Meteor. Soc.*, *126*, 889-898.

Raymond, D. J. (2001). A new model of the Madden-Julian oscillation. *J. Atmos. Sci.*, *58*, 2807-2819.

Raymond, D. J. (2007). Testing a cumulus parametrization with a cumulus ensemble model in weak-temperature-gradient mode. *Quart. J. Roy. Meteor. Soc.*, *133*, 1073-1085.

Raymond, D. J. (2012). Balanced thermal structure of an intensifying tropical cyclone. *Tellus*, *64*, 19181, doi:org/10.3402/tellusa.v64i0.19181.

Raymond, D. J. (2013). Sources and sinks of entropy in the atmosphere. *J. Adv. Model. Earth Syst.*, *5*, 755-763, doi:10.1002/jame.20050.

Raymond, D. J. (2017). Convection in the east Pacific intertropical convergence zone. *Geophys. Res. Lett.*, *44*, 562-568, doi:10.1002/2016GL071554.

Raymond, D. J., G. B. Raga, C. S. Bretherton, J. Molinari, C. López-Carrillo and Ž. Fuchs (2003). Convective forcing in the intertropical convergence zone of the eastern Pacific. *J. Atmos. Sci.*, *60*, 2064-2082.

Raymond, D. J., C. S. Bretherton and J. Molinari (2006). Dynamics of the intertropical convergence zone of the east Pacific. *J. Atmos. Sci.*, *63*, 582-597.

Raymond, D. J., S. L. Sessions and Ž. Fuchs (2007). A theory for the spinup of tropical depressions. *Quart. J. Roy. Meteor. Soc.*, *133*, 1743-1754.

Raymond, D. J., S. Sessions, A. Sobel and Ž. Fuchs (2009). The mechanics of gross moist stability. *J. Adv. Model Earth Syst.*, *1 #9*, 20 pp.

Raymond, D. J., S. L. Sessions and C. López-Carrillo (2011). Thermodynamics of tropical cyclogenesis in the northwest Pacific. *J. Geophys. Res.*, *116*, D18101, doi:10.1029/2011JD015624.

Raymond, D. J., S. Gjorgjievska, S. Sessions and Ž. Fuchs (2014). Tropical cyclogenesis and mid-level vorticity. *Australian Meteorological and Oceanographic Journal*, *64*, 11-25.

Raymond, D. J., Ž. Fuchs, S. Gjorgjievska and S. L. Sessions (2015). Balanced dynamics and convection in the tropical troposphere. *J. Adv. Model. Earth Syst.*, *7*, doi:10.1002/2015MS000467.

Raymond, D. J. and M. M. Flores (2016). Predicting convective rainfall over tropical oceans from environmental conditions. *J. Adv. Model. Earth Syst.*, *8*, doi:10.1002/2015MS000595.

Raymond, D. J. and Ž. Fuchs (2009). Moisture modes and the Madden-Julian oscillation. *J. Climate*, *22*, 3031-3046.

Raymond, D. J. and G. Kilroy (2019). Control of convection in high-resolution simulations of tropical cyclogenesis. *J. Adv. Model. Earth Syst.*, *11*, 1582-1599.

Raymond, D. J. and C. López-Carrillo (2011). The vorticity budget of developing typhoon Nuri (2008). *Atmos. Chem. Phys.*, *11*, 147-163.

Raymond, D. J. and S. L. Sessions (2007). Evolution of convection during tropical cyclogenesis. *Geophys. Res. Lett.*, *34*, L06811, doi:10.1029/2006GL028607.

Sentić, S, S. L. Sessions, and Ž. Fuchs (2015). Diagnosing DYNAMO convection with weak temperature gradient simulations. *J. Adv. Model. Earth Syst.*, *7*, doi:10.1002/2015MS000531.

Sessions, S. L., M. J. Herman and S. Sentić (2015). Convective response to changes in the thermodynamic environment in idealized weak temperature gradient simulations. *J. Adv. Model. Earth Syst.*, *7*, 712-738, doi:10.1002/2015MS000446.

Sherwood, S. C. (1999). Convective precursors and predictability in the tropical western Pacific. *Mon. Wea. Rev.*, *127*, 2977-2991.

Shi, X., D. Kim, Á. F. Adames and J. Sukhatme (2018). WISHE-moisture mode in an aquaplanet simulation. *J. Adv. Model. Earth Syst.*, *10*, 2393-2407.

Singh, M. S. and P. A. O'Gorman (2013). Influence of entrainment on the thermal stratification in simulations of radiative-convective equilibrium. *Geophys. Res. Lett.*, *40*, 4398-4403.

Sobel, A. and E. Maloney (2012). An idealized semi-empirical framework for modeling the Madden-Julian oscillation. *J. Atmos. Sci.*, *69*, 1691-1705.

Sobel, A. and E. Maloney (2013). Moisture modes and the eastward propagation of the MJO. *J. Atmos. Sci.*, *70*, 187-192.

Stevens, B., J. Duan, J. C. McWilliams, M. Munnich and J. D. Neelin (2002). Entrainment, Rayleigh friction, and boundary layer winds over the tropical Pacific. *J. Climate*, *15*, 30-44.

Thayer-Calder, K. and D. Randall (2015). A numerical investigation of boundary layer quasi-equilibrium. *Geophys. Res. Lett.*, *42*, doi:10.1002/2014GL062649.

UCAR/NCAR - Earth Observing Laboratory, Voemel, H. (2019). NCAR/EOL AVAPS Dropsonde QC Data. Version 1.0. UCAR/NCAR - Earth Observing Laboratory `https://doi.org/10.26023/EHRT-TN96-9W04`. Accessed 27 January 2020.

Zipser, E. J. (1969). The role of organized unsaturated convective downdrafts in the structure and rapid decay of an equatorial disturbance. *J. Appl. Meteor.*, *8*, 799-814.

Zipser, E. J. (1977). Mesoscale and convective scale downdrafts as distinct components of squall-line structure. *Mon. Wea. Rev.*, *105*, 1568-1589.